Lateral instability of stationary spherical reaction balls

Ágota Tóth, Péter Kevei, and Dezső Horváth*
Department of Physical Chemistry, University of Szeged, P.O. Box 105, Szeged, H-6701, Hungary
(Received 29 May 2006; published 28 September 2006)

Three-dimensional stability of stationary reaction balls is investigated in a system consisting of an autocatalysis accompanied by a slow decay of the autocatalyst. Radially stable stationary spherical structures become unstable to three-dimensional perturbations at small decay rate when the radius of the reaction ball is sufficiently large and the reactant diffuses faster than the autocatalyst. A thorough linear stability analysis and simulations in three spatial dimensions are carried out in the simplest system sustaining stationary reaction balls.

DOI: 10.1103/PhysRevE.74.036214 PACS number(s): 89.75.Kd, 47.54.−r, 02.30.Mv, 82.33.Vx

I. INTRODUCTION

In a chemical reaction containing an autocatalytic step, a reaction front may be initiated by a local input of the autocatalyst in a spatially extended unstirred system. The front—defined as the thin layer where the reactants are converted into products at significant rate—then propagates into the unreacted fresh zone as a result of the coupling between autocatalysis and diffusion [1–3]. The latter is the only mass transport process considered in this work. The velocity of front propagation therefore greatly depends on the diffusion coefficient of the key species: the greater the diffusion rate of the autocatalyst, the faster the reaction front propagates forward [4].

In a simple autocatalytic system consisting of an autocatalytic step followed by a decay of the autocatalyst according to

$$A + pB \rightarrow (p+1)B, \quad \text{rate}_1 = k_1 a b^p \quad (p > 5), \tag{1}$$

$$B \rightarrow C, \quad \text{rate}_2 = k_2 b, \tag{2}$$

the velocity of a spherical reaction front propagating outward in the three-dimensional space may drop to zero when the autocatalyst diffuses at a slower rate than the reactant [5]. The resultant time-independent structure can be viewed as a localized reactor where the final product (C) is formed, which then diffuses out as long as there is sufficient fresh reactant around. The existence of this stationary spherical structure has been shown in previous studies [5,6], in which it has also been termed as an isothermal flame ball [5,6], since it may be considered as an analogy to a flame ball existing in premixed laminar flames [7,8]. In combustion, the positive feedback is provided by the exothermic reaction via the Arrhenius-type temperature dependence, while the evolved heat is released from the ball via radiation [9]. Due to the immense increase in temperature, flame balls have only been observed in the absence of gravitation where convective motion does not occur [10].

At very slow rate of autocatalyst decay with respect to that of autocatalyst production, the radius of the stationary reaction ball becomes large [5]. At this scenario lateral instability may be anticipated, since the reactant must have greater diffusion coefficient in order to observe radially stable spherical structures. This relation between the diffusion coefficients favors the evolution of transverse instability in systems where the order of autocatalysis is greater than two in the absence [11,12] or even in the presence [13] of a slow autocatalyst decay.

This issue of transverse instability within the domain of existing stationary spherical reaction front is addressed in this work, where we carry out a thorough three-dimensional linear stability analysis of the time-independent structure by calculating the temporal eigenvalues for the most important spatial modes. We are interested in identifying parameter ranges where the instability arises and at the same time the reaction ball is stable to radial perturbation. We also carry out simulations in the three-dimensional space to visualize the patterns appearing beyond the onset of instability. The thin front approximation applied in an earlier work [13] is not carried out as the slow autocatalyst decay is not negligible ahead of the reaction front, i.e., outside the reaction ball, similarly to flame balls with far field heat losses [8].

II. MODELING STUDY

The equations governing the reaction-diffusion system based on Eqs. (1) and (2) are

$$\frac{\partial a}{\partial t} = D_A \nabla^2 a - k_1 a b^p, \tag{3}$$

$$\frac{\partial b}{\partial t} = D_B \nabla^2 b + k_1 a b^p - k_2 b, \tag{4}$$

where a and b are the concentrations, D_A and D_B are the diffusion coefficients of A and B, respectively. Boundary conditions are selected as

$$a \rightarrow a_0, \quad b \rightarrow 0 \quad \text{as } |\mathbf{x}| \rightarrow \infty, \tag{5}$$

representing only reactant A sufficiently far from the reaction zone. For spherical reaction balls the initial conditions implicitly defined as

$$a = a_0, \quad b = 0 \quad \text{at } t = 0 \quad \text{for all } \mathbf{x}, \tag{6}$$

i.e., a homogeneous distribution of pure reactant A exists apart from a local region, centered at the origin, where there

*Email: horvathd@chem.u-szeged.hu

is some input of autocatalyst B to initiate a reaction.

For simplification, we introduce dimensionless concentrations $\alpha=a/a_0$ and $\beta=b/a_0$ with respect to the initial concentration of reactant A leading to

$$\frac{\partial \alpha}{\partial \tau} = \nabla^2 \alpha - \alpha \beta^p, \tag{7}$$

$$\frac{\partial \beta}{\partial \tau} = D\nabla^2 \beta + \alpha \beta^p - \kappa \beta, \tag{8}$$

where $D=D_B/D_A$ is the ratio of diffusion coefficients and $\kappa=k_2/(k_1 a_0^p)$ is the decay rate of B with respect to the rate of autocatalysis. The dimensionless time and length scales are then defined as $\tau=(k_1 a_0^p)t$ and, $\bar{\mathbf{x}}=\mathbf{x}\sqrt{k_1 a_0^p/D_A}$, respectively.

Since we are interested in the stability of a spherical reaction front, it is convenient to express $\bar{\mathbf{x}}$ in terms of polar coordinates r, θ, and ϕ; hence in Eqs. (7) and (8) ∇^2 is rewritten as

$$\nabla^2 = \frac{1}{r^2}\frac{\partial}{\partial r}\left(r^2 \frac{\partial}{\partial r}\right) + \frac{1}{r^2 \sin\theta}\frac{\partial}{\partial \theta}\left(\sin\theta \frac{\partial}{\partial \theta}\right) + \frac{1}{r^2 \sin^2\theta}\frac{\partial^2}{\partial \phi^2}. \tag{9}$$

Previously it has been shown that in case of stationary reaction balls the time-independent solution itself may be characterized by a single parameter $K=D^{p-1}\kappa$ by rescaling the radial part of Eqs. (7) and (8) [5]. We can introduce $\tilde{\beta}=D\beta$ and $\tilde{r}=r/\sqrt{D^p}$ to obtain

$$0 = \frac{d^2\alpha}{d\tilde{r}^2} + \frac{2}{\tilde{r}}\frac{d\alpha}{d\tilde{r}} - \alpha\tilde{\beta}^p, \tag{10}$$

$$0 = \frac{d^2\tilde{\beta}}{d\tilde{r}^2} + \frac{2}{\tilde{r}}\frac{d\tilde{\beta}}{d\tilde{r}} + \alpha\tilde{\beta}^p - K\tilde{\beta}, \tag{11}$$

where the gradients vanish at the boundary $\tilde{r}=0$. The stability of the stationary structure and the temporal evolution of concentrations will, however, also depend on the ratio of diffusion coefficients D.

For the stability analysis the perturbation is introduced in the form of

$$\alpha(\tau,r,\theta,\phi) = \alpha_0(r) + \alpha_1(r)T(\tau)Y(\theta,\phi), \tag{12}$$

$$\beta(\tau,r,\theta,\phi) = \beta_0(r) + \beta_1(r)T(\tau)Y(\theta,\phi), \tag{13}$$

where α_0 and β_0 represent the spherical reaction ball, i.e., the solution of Eqs. (10) and (11) scaled back to r. Upon substituting Eqs. (12) and (13) into Eq. (7) and considering the terms first order with respect to the perturbation, we obtain

$$\alpha_1 Y T_\tau = \left((\alpha_1)_{rr} + \frac{2}{r}(\alpha_1)_r\right)TY + \frac{\alpha_1 T Y_{\theta\theta}}{r^2} + \frac{\alpha_1 T Y_\theta \cos\theta}{r^2 \sin\theta} + \frac{\alpha_1 T Y_{\phi\phi}}{r^2 \sin^2\theta} - p\alpha_0\beta_1 T Y \beta_0^{p-1} - \alpha_1 \beta_0^p T Y, \tag{14}$$

where variables in the lower index represent differentiation with respect to them. A division by $\alpha_1 YT$ yields

$$\frac{T_\tau}{T} = \frac{(\alpha_1)_{rr} + 2(\alpha_1)_r/r}{\alpha_1} + \frac{Y_{\theta\theta}}{r^2 Y} + \frac{Y_\theta \cos\theta}{r^2 Y \sin\theta} + \frac{Y_{\phi\phi}}{r^2 Y \sin^2\theta} - \frac{p\alpha_0\beta_1\beta_0^{p-1}}{\alpha_1} - \beta_0^p. \tag{15}$$

The left-hand side of the equation is a function of time, while the right-hand side depends only on the spatial coordinates, therefore they are both equal to a constant (ω). The radial coordinate can be separated from the angular coordinates by rearranging the right-hand side of Eq. (15) as

$$\omega r^2 - \frac{r^2(\alpha_1)_{rr} + 2r(\alpha_1)_r}{\alpha_1} + \frac{r^2 p\alpha_0\beta_1\beta_0^{p-1}}{\alpha_1} + r^2\beta_0^p = \frac{1}{Y}\left(Y_{\theta\theta} + \frac{\cos\theta}{\sin\theta}Y_\theta + \frac{Y_{\phi\phi}}{\sin^2\theta}\right), \tag{16}$$

where again both sides must be equal to a constant ($-B$). The angular part in the form of

$$\sin\theta\frac{\partial}{\partial\theta}(Y_\theta \sin\theta) + Y_{\phi\phi} + BY\sin^2\theta = 0 \tag{17}$$

is the equation defining the spherical harmonics, which has a solution only when $B=l(l+1)$, where $l\geqslant 0$ is an integer. We can now formulate the first equation for the radial part of the perturbation as

$$\omega\alpha_1 = \frac{d^2\alpha_1}{dr^2} + \frac{2}{r}\frac{d\alpha_1}{dr} - \frac{l(l+1)\alpha_1}{r^2} - \beta_0^p\alpha_1 - p\alpha_0\beta_0^{p-1}\beta_1. \tag{18}$$

Following the same arguments we can obtain

$$\omega\beta_1 = D\left(\frac{d^2\beta_1}{dr^2} + \frac{2}{r}\frac{d\beta_1}{dr} - \frac{l(l+1)\beta_1}{r^2}\right) + \beta_0^p\alpha_1 + p\alpha_0\beta_0^{p-1}\beta_1 - \kappa\beta_1. \tag{19}$$

The eigenvalue-problem defined in Eqs. (18) and (19) characterizes the stability of stationary spherical reaction balls. Lateral instability occurs when $\mathrm{Re}(\omega)$ becomes positive for $l>0$ while the structure is radially stable [$\mathrm{Re}(\omega)$ is negative for $l=0$].

In order to solve Eqs. (18) and (19), it is imperative to identify the boundary conditions. It can be readily shown that when $r=0$, $\alpha_1=\beta_1=0$ for $l\geqslant 1$, while $d\alpha_1/dr=d\beta_1/dr=0$ for $l=0$. Since the perturbation is localized to the reaction front, both α_1 and β_1, along with their gradients, tend to zero as $r\to+\infty$.

III. NUMERICAL METHODS

The concentration profiles of the stationary spherical reaction balls are the solutions of the two-point boundary value problem defined in Eqs. (10) and (11), and are obtained by a shooting method for $p=6$ in the (α, $\tilde{\beta}$, $d\alpha/d\tilde{r}$, $d\tilde{\beta}/d\tilde{r}$) phase space as described in details in Ref. [5]. The values of α and $\tilde{\beta}$ at $\tilde{r}=0$ are varied in an iterative manner until the calculated trajectory matches the asymptotic functions as

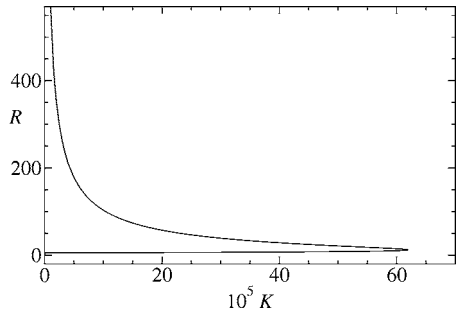

FIG. 1. Radius of reaction ball as a function of the rate of autocatalyst decay with relative to the autocatalysis. The radius (in $\tilde{r}$) is defined as that of the spherical shell where the rate of autocatalysis is at maximum in the stationary structure.

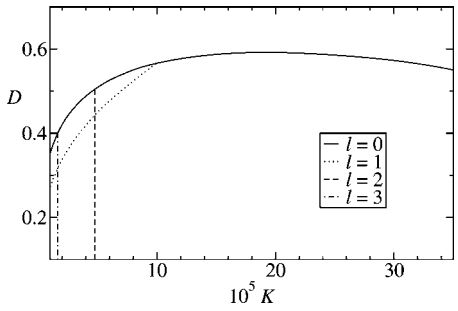

FIG. 2. Phase diagram for the upper branch in Fig. 1 for systems with reactant A having greater diffusion coefficient than autocatalyst B. The solid line separates reaction balls unstable (above) or stable (below) to radial, i.e., one-dimensional, perturbation. Dashed and dotted lines mark the onset of instability to three-dimensional perturbation as K is decreased for various l values.

$\tilde{r}\to+\infty$. The numerical integration is carried out by using the CVODE package [14].

The first-order perturbation is solved by discretizing Eqs. (18) and (19), which yields the eigenvalue problem

$$\omega\begin{pmatrix}\vdots\\ \alpha_{1,i}\\ \beta_{1,i}\\ \vdots\end{pmatrix}=L\begin{pmatrix}\vdots\\ \alpha_{1,i}\\ \beta_{1,i}\\ \vdots\end{pmatrix}, \tag{20}$$

where matrix L is constructed from the discretized concentration profiles obtained from the shooting for selected decay rate of the autocatalyst K, ratio of the diffusion coefficients D, and spatial wave number l associated with the spherical harmonics. The DGEEV routine of LAPACK [15] is then used to calculate the eigenvalues and eigenvectors of the 1002×1002 matrix.

A three-dimensional calculation is also carried out by integrating Eqs. (7) and (8) for $p=6$ on a $201\times201\times201$ cubic grid with uniform spacing of $h=0.01-0.024$. The Laplacian is approximated with a 27-point formula as

$$\nabla^2 c_{i,j,k}\approx\frac{1}{6h^2}\sum_{r=-1,s=-1,t=-1}^{+1,+1,+1}A_{r,s,t}c_{i+r,j+s,k+t}, \tag{21}$$

where $A_{\pm1,\pm1,\pm1}=0$, $A_{0,\pm1,\pm1}=A_{\pm1,0,\pm1}=A_{\pm1,\pm1,0}=1$, $A_{0,0,\pm1}=A_{\pm1,0,0}=A_{0,\pm1,0}=2$, and $A_{0,0,0}=-24$, resulting in an error of $O(h^2)$ [16]. An explicit Euler method is applied at the iteration steps with $\Delta\tau=1\times10^{-5}-6\times10^{-5}$. The grid spacing is selected so that the total size of the grid allows the application of the asymptotic functions in Ref. [5] around the grid as boundary conditions. For initial conditions, one or two protuberances are placed on the spherical concentration profiles obtained by shooting in the radial system, followed by the addition of a small random noise in the concentration of the autocatalyst B.

IV. RESULTS AND DISCUSSION

We have selected the system with the smallest order of autocatalysis ($p=6$) that exhibits stationary spherical structures, for which Eqs. (10) and (11) have two solutions for $K<6.190\,249\times10^{-4}$ as shown in Fig. 1 [5], where the solutions are characterized by their radius defined as $\tilde{r}$ at the maximum rate of the autocatalytic step. The lower branch represents the critical size of initiation below which front propagation fails and the system returns to the original unreacted states containing only A.

At equal diffusivities no stable stationary reaction balls exist. The upper branch in Fig. 1 may be radially stabilized by increasing the flux of the reactant with respect to that of the autocatalyst. The stable spherical structure appears at $D=0.592$ in the middle of the branch and the range of stability rapidly grows as the diffusion coefficient of autocatalyst B decreases as shown by the solid line in Fig. 2. The change of stability for $l=0$ at the right end of the region has been shown to occur via a Hopf bifurcation previously [5]. Our stability analysis reveals that the same scenario occurs at the left end of the stable region (at smaller K).

With decreasing K, the radius of the reaction ball significantly increases (cf. Fig. 1), therefore lateral instability of the reaction front may be anticipated as the curvature decreases, since the diffusion coefficient of reactant A is greater than that of the autocatalyst. For $l=1$ the loss of stability occurs via a Hopf bifurcation at $K<9.97\times10^{-5}$, while for $l=2$, or $l=3$ the instability arises as saddle-node bifurcations at $K=4.77\times10^{-5}$ and $K=1.63\times10^{-5}$, respectively. As Fig. 2 clearly shows, the onset of instability is independent of the ratio of diffusion coefficients D for $l>1$, leaving K as the sole parameter to determine the stability. Although the first-order perturbation in Eqs. (18) and (19) depends on both D and K, at the saddle-node bifurcation (when $\omega=0$), D can be scaled out similarly to the time-independent solution in Eqs. (10) and (11), resulting in

$$0=\frac{d^2\alpha_1}{d\tilde{r}^2}+\frac{2}{\tilde{r}}\frac{d\alpha_1}{d\tilde{r}}-\frac{l(l+1)\alpha_1}{\tilde{r}^2}-\tilde{\beta}_0{}^p\alpha_1-p\alpha_0\tilde{\beta}_0{}^{p-1}\tilde{\beta}_1,$$

$$0=\frac{d^2\tilde{\beta}_1}{d\tilde{r}^2}+\frac{2}{\tilde{r}}\frac{d\tilde{\beta}_1}{d\tilde{r}}-\frac{l(l+1)\tilde{\beta}_1}{\tilde{r}^2}+\tilde{\beta}_0{}^p\alpha_1+p\alpha_0\tilde{\beta}_0{}^{p-1}\tilde{\beta}_1-K\tilde{\beta}_1.$$

In the three-dimensional simulations when the temporal eigenvalues have negative real parts for all spatial modes, the initial perturbations decay and the stable stationary spherical

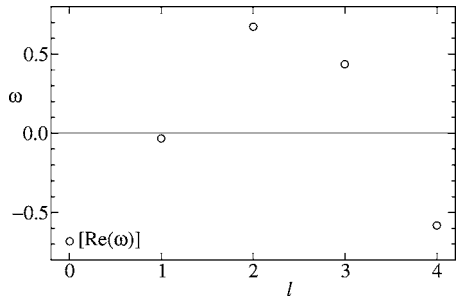

FIG. 3. Dispersion relation at $K=1.0\times10^{-5}$ and $D=0.1$ for the reaction ball on the upper branch of Fig. 1 ($R=578$).

structure is retained in accordance with the phase diagram shown in Fig. 2. With decay rate less than the onset of instability, where the radius of the reaction ball is greater, the perturbations will distort the spherical symmetry by producing one or two protuberances on the reaction ball. Further away from the onset of instability, the splitting of the reaction ball may be observed as presented in an example case in Fig. 3, where the temporal eigenvalue ω takes on a positive value for $l=2$ and $l=3$ only. The spherical structure, stable in the one-dimensional radial system [since $\mathrm{Re}(\omega)<0$ for $l=0$], is now unstable to angular perturbation. Depending on the initial spatial distribution of the perturbation, the spherical structure breaks into two to three lobes that separate from each other. The separated front segments may then further divide as shown in Fig. 4, where black regions represent high concentration of autocatalyst B.

In conclusion, we have shown that in the simplest model system able to sustain stationary spherical structures, termed reaction balls, instability to three-dimensional perturbation arises at slow decay rate of the autocatalyst when the radius of the stationary reaction ball is large. The phenomenon is an analogy to the lateral instability of planar reaction front; it also occurs when the diffusion coefficient of the reactant is greater than that of the autocatalyst. In the unstable region, the perturbed reaction balls exhibit consecutive expansion and splitting also observed in simulations of spherical premixed flames [17]. The large order required for the existence of stable spherical structures may seem extraordinary, however, there are examples of complex reactions of inorganic ions [18], micellar autocatalysis [19], and polymerization of sickle hemoglobin [20] where very high order has been observed.

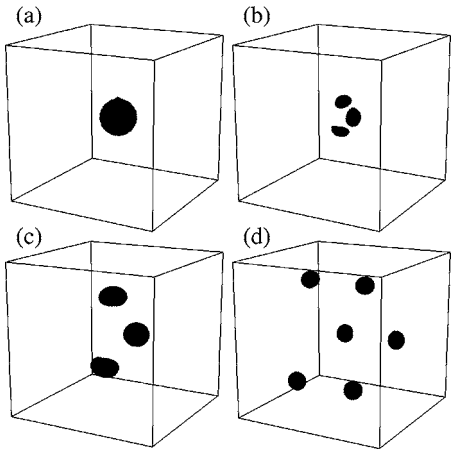

FIG. 4. Temporal evolution of a perturbed spherical reaction ball with parameters listed under Fig. 3. Black regions represent volumes of high autocatalyst concentration (above 90% of the maximum value). Time after perturbation $\tau=0$ (a), 6(b), 12(c), 24(d).

ACKNOWLEDGMENT

This work was supported by the Hungarian Scientific Research Fund (Grant No. OTKA T046010).

[1] G. Nicholis and I. Prigogine, *Self-Organization in Nonequilibrium Chemical Systems* (Wiley, New York, 1977).
[2] *Chemical Waves and Patterns*, edited by R. Kapral and K. Showalter (Kluwer, Dordrecht, 1995).
[3] I. R. Epstein and K. Showalter, J. Phys. Chem. **100**, 13132 (1996).
[4] S. K. Scott and K. Showalter, J. Phys. Chem. **96**, 8702 (1992).
[5] É. Jakab, D. Horváth, J. H. Merkin, S. K. Scott, P. L. Simon, and Á. Tóth, Phys. Rev. E **68**, 036210 (2003).
[6] É. Jakab, D. Horváth, J. H. Merkin, S. K. Scott, P. L. Simon, and Á. Tóth, Phys. Rev. E **66**, 016207 (2002).
[7] Y. B. Zeldovich, *Theory of Combustion and Detonation of Gases* (Academy of Sciences, Moscow, 1944).
[8] J. D. Buckmaster, G. Joulin, and P. D. Ronney, Combust. Flame **84**, 411 (1991).
[9] J. D. Buckmaster, M. Smooke, and V. Giovangigli, Combust. Flame **94**, 113 (1993).
[10] P. D. Ronney, K. N. Whaling, A. Abbud-Madrid, J. L. Gatto, and V. L. Pisowicz, AIAA J. **32**, 569 (1994).
[11] D. Horváth, V. Petrov, S. K. Scott, and K. Showalter, J. Chem. Phys. **98**, 6332 (1993).
[12] W. van Saarloos, Phys. Rep. **386**, 29 (2003).
[13] Á. Tóth, D. Horváth, É Jakab, J. H. Merkin, and S. K. Scott, J. Chem. Phys. **114**, 9947 (2001).
[14] S. D. Cohen and A. C. Hindmarsh, Comput. Phys. **10**, 138 (1996).
[15] E. Anderson *et al.*, *LAPACK Users' Guide* (Society for Industrial and Applied Mathematics, Philadelphia, 1999).
[16] M. Dowle, R. M. Mantel, and D. Barkley, Int. J. Bifurcation Chaos Appl. Sci. Eng. **7**, 2529 (1997).
[17] W. Gerlinger, K. Schneider, J. Fröhlich, and H. Bockhorn, Combust. Flame **132**, 247 (2003).
[18] A. K. Horváth, I. Nagypál, G. Peintler, and I. R. Epstein, J. Am. Chem. Soc. **126**, 6246 (2004).
[19] T. Buhse, R. Nagarajan, D. Lavabre, and J. C. Micheau, J. Phys. Chem. A **101**, 3910 (1997).
[20] F. A. Ferrone, J. Hofrichter, and W. A. Eaton, J. Mol. Biol. **183**, 591 (1985).